

# Quantifying the Diffusion of a Fluid through Membranes by Double Phase Encoded Remote Detection Magnetic Resonance Imaging

Ville-Veikko Telkki,\* Christian Hilty,<sup>§</sup> Sandra Garcia, Elad Harel, and Alexander Pines

Materials Sciences Division, Lawrence Berkeley National Laboratory, and Department of Chemistry, University of California at Berkeley, Berkeley, California 94720-1460

Received: August 23, 2007; In Final Form: October 17, 2007

We demonstrate that a position correlation magnetic resonance imaging (MRI) experiment based on two phase encoding steps separated by a delay can be used for quantifying diffusion across a membrane. This method is noninvasive, and no tracer substance or concentration gradient across the membrane is required. Because, in typical membranes, the  $T_1$  relaxation time of the fluid spins is usually much longer than the  $T_2$  time, we developed and implemented a new position correlation experiment based on a stimulated spin-echo, in which the relaxation attenuation of the signal is dominated by  $T_1$  instead of  $T_2$ . This enables using relatively long delays needed in the diffusion measurements. The sensitivity of the double encoded experiment detected in a conventional way is still low because of the low filling factor of the fluid inside the NMR coil around the sample. We circumvent this problem by using the remote detection technique, which significantly increases the sensitivity, making it possible to do the measurements with gaseous fluids that have a low spin-density compared to liquids. We derive a model that enables us to extract a diffusion constant characterizing the diffusion rate through the membrane from the obtained correlation images. The double phase encoded MRI method is advantageous in any kind of diffusion studies, because the propagator of fluid molecules can directly be seen from the correlation image.

## 1. Introduction

In this article, we introduce a novel method for measuring the diffusion of fluids across membranes. Membranes are of paramount importance in science and technology, for example, for fuel cells,<sup>1</sup> for the purification of water,<sup>2</sup> gas separation,<sup>3</sup> or metabolism.<sup>4</sup> Present methods for the characterization of diffusion across membranes typically rely on the determination of the change in concentration or partial pressure of the fluid in a system that is in nonequilibrium at the beginning of the measurement. Alternatively, radioactive nuclei that are incorporated into the diffusing compounds are sometimes used as tracers.<sup>5</sup> However, in the former case, the dependence of the diffusion coefficient on concentration may lead to results that differ from the equilibrium values, whereas, in the latter case, the labeling is often chemically challenging, and the difference in mass between labeled and unlabeled molecules may affect results.<sup>5</sup>

Pulsed-field-gradient spin-echo (PGSE)<sup>6</sup> and its variant pulsed-field-gradient *stimulated* echo (PGSTE)<sup>7</sup> nuclear magnetic resonance (NMR) experiments are widely used for measuring the bulk diffusion of fluids. The basic idea of these experiments is that, if the molecules are fixed in space during the delay between two magnetic field gradient pulses, they form a perfect echo, and the longer the distance the molecules travel during the delay, the smaller the amplitude of the echo. In the PGSE pulse sequence, the gradient pulses are before and after a  $\pi$  radio frequency (rf) pulse of a spin-echo sequence. PGSTE

comprises three  $\pi/2$  rf pulses, and the gradient pulses are between the first two rf pulses and after the last one. The second rf pulse stores one component of magnetization as a longitudinal magnetization, preventing dephasing during the delay between the second and third rf pulses. Hence, the major difference between PGSE and PGSTE experiments is that relaxation attenuation of the signal is dominated by  $T_2$  in the former case, whereas it is  $T_1$  in the latter case. When  $T_1$  is substantially larger than  $T_2$ , the sensitivity in the PGSTE experiment is better, even though one component of the magnetization vector is lost in the storage of magnetization.

PGSE and PGSTE methods have also been used for studying the diffusion of fluids in restricted systems such as in porous media where measurements can reveal important parameters characteristic of the material such as pore size and connectivity.<sup>8–10</sup> There are several different approaches for this kind of study. One approach is to study the echo amplitude in a wide range of  $q$  values ( $q = \gamma\delta g$ , where  $\gamma$  is the gyromagnetic ratio,  $\delta$  is the length of the gradient pulse, and  $g$  is the gradient amplitude) in the long diffusion time limit.<sup>11–13</sup> Another is to determine the effective diffusion coefficient in the low  $q$  region as a function of diffusion time.<sup>14–16</sup> These experiments are advantageous in the case of homogeneous systems with a periodic lattice, because they measure the average of the properties of the whole system, and, in principle, the sensitivity scales with the size of the sample. However, this advantage fails if the diffusion across a single membrane is studied.

Here, we present a direct measurement of membrane permeability by a distinct method using magnetic resonance imaging (MRI). A conventional MRI experiment contains only one encoding step, in which the positional information of the molecules is encoded in the spin coherences. In contrast, our pulse sequence uses two encoding steps separated by a delay.

\* Corresponding author. Current address: NMR Research Group, Department of Physical Sciences, University of Oulu, P. O. Box 3000, FIN-90014 Oulu, Finland. Phone: +358 8 553 1309. Fax: +358 8 5531287. E-mail: ville-veikko.telkki@oulu.fi.

<sup>§</sup> Current address: Department of Chemistry, Texas A&M University, College Station, Texas 77843.

The double encoding allows correlating the initial and final positions of the molecules. Hence, the propagator, that is, the positional distribution of molecules being at certain position in the beginning of the experiment (during the first encoding step) and in the end of the experiment (during the second encoding step), can be directly seen from a two-dimensional correlation image, without using the relatively complicated models needed in the analysis of results of PGSE and PGSTE experiments.

It is difficult to find a geometric arrangement of a membrane with respect to an NMR coil so that the sample fills the entire coil. In our case, the actual sample is approximately 500 times smaller than the NMR coil, giving rise to a considerable sensitivity problem. We circumvent this problem by using the remote detection technique developed in our lab. Remote detection of NMR spatially separates the encoding and detection steps of the experiment, enabling the separate optimization of each step.<sup>17–22</sup> In this study, we use a large coil around the sample for encoding the spin coherences, and the signal is detected by a much smaller and more sensitive detection coil (solenoid) with an optimized filling factor. The flow of a probe fluid transports the signal from the sample region to the detector. Apart from sensitivity enhancement, the remote detection technique provides time-of-flight (TOF) information of the fluid molecules as they flow from the encoding region to the detector, making it possible to get three-dimensional TOF images of the flowing fluid.<sup>17</sup> Here, we use TOF flow images for measuring the flow rate and selecting the signal only from the membrane region in the diffusion measurements.

We use xenon gas as a probe fluid in this demonstration. Xenon is frequently used for characterizing porous media,<sup>23</sup> and it allows for hyperpolarization to boost the obtainable NMR signal.<sup>24,25</sup> Apart from the hyperpolarization, the long  $T_1$  relaxation time of xenon makes it a favorable choice for a probe fluid in the remote detection experiments, because the loss of signal due to relaxation during the flow from the encoding region to the detection region is minimal.

## 2. Experimental Section

Two different ANOPORE inorganic aluminum oxide membranes manufactured by Structure Probe, Inc. (West Chester, PA) were studied. They contained straight, parallel pores with the pore axis perpendicular to the surface of the membrane. According to the manufacturer, the pore diameters of the membranes were 20 and 200 nm, and the thickness of both membranes was 60  $\mu\text{m}$ . The surface porosities of the 20 and 200 nm membranes were 50% and 25–30%, respectively. On the basis of the images of the membranes provided by the manufacturer, it can be deduced that the pore size distribution is relatively narrow, and there are no dead-end pores in the membranes.

In the measurements, the membrane was set in the center of the flow channel along the long axis of the channel. The cross section of the channel was square. The width and length of the channel were 1.2 mm and 3 cm, respectively. Probe gas flowed parallel to the surface of the membrane, and the pressure was equal on both sides of the membrane. The flow direction ( $z$ ) and the direction in which diffusion was studied ( $y$ ) were perpendicular to each other. The latter direction was parallel to the pore axes. The schematic of the experimental setup is shown in Figure 1. The details of the sample holder are illustrated in Figure 2.

In the remote detection experiments, the encoding was done by a commercial imaging probe (Varian, Inc., Palo Alto, CA) with a cylindrical cavity (3 cm in diameter) along its full length.

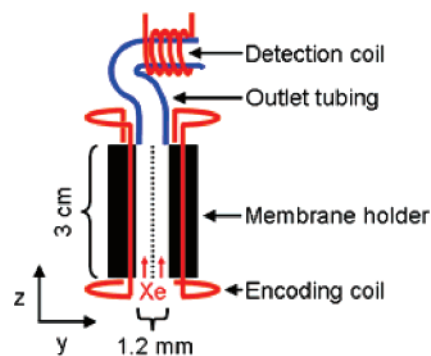


**Figure 1.** Schematic of the experimental setup. The holder containing the flow channel is inside the encoding coil. The membrane is set in the center of the channel, and xenon gas flows parallel to its surface (upward). The detection coil is wrapped around the outlet tubing. The used frame of reference is shown in the figure. The membrane is in the  $xz$  plane, xenon gas flows in the  $z$  direction, and diffusion is measured along the  $y$ -axis.

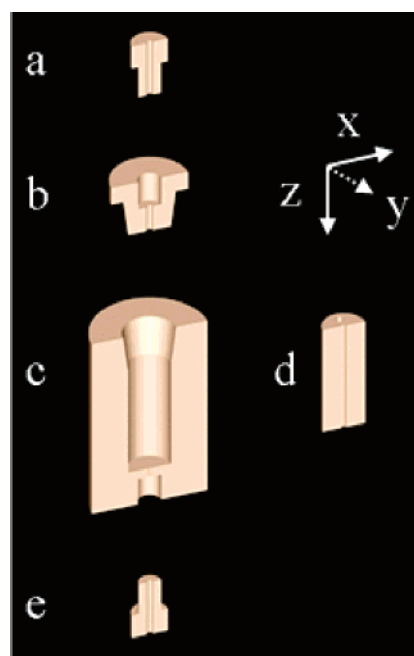


**Figure 2.** A cross section of the membrane holder. The 1/16'' (1.6 mm) o.d. inlet tubing was connected with a fitting (a) to a plug (b), which was screwed into the actual sample holder (c). The height and diameter of the holder were 5 and 3 cm, respectively. The holder contained a cylindrical chamber, and the membrane was placed along the center axis of the chamber, squeezed between two half cylinders (d) (length 3 cm, diameter 1.1 cm). The flow channel was milled into the flat surfaces of the half cylinders. Gas flowed through a small hole from the chamber to a fitting connected to the outlet tubing with 1/16'' (1.6 mm) o.d. (e).

The height of the coil of the imaging probe was 4 cm. A home-built detection probe was pushed from underneath into the cavity so that the detection coil was about 1.5 cm below the imaging coil region. The detection coil (solenoid) was wrapped around 1/16'' (1.6 mm) outside diameter (o.d.) outlet tubing, and the length of the coil was about 5 mm. The rf isolation between the two probes was achieved with a grounded copper shield. More information about the design of the detection probe can be found from refs 26 and 27. The MRI experiments were performed on a Unity Inova 300 MHz spectrometer (Varian, Inc.), in which the xenon resonance frequency is 82.9 MHz. In all the remote detection experiments, the acquisition time of one free induction decay (FID) was 40 ms (which is also the

time resolution in TOF experiments), and 50 consecutive FIDs were collected during one scan, leading to a total acquisition time of 2 s per transient. The length of the gradient pulses was 200  $\mu\text{s}$ . In the  $z$  encoded TOF experiment, the maximum gradient amplitude and the field of view were 9.7 G/cm and 5 cm, respectively. In the  $yz$  encoded TOF experiment, the corresponding values in the  $y$  direction were 60 G/cm and 2.1 mm, and in the  $z$  direction, they were 2.5 G/cm and 5 cm. In the  $yy$  encoded diffusion experiment, the values were 60 G/cm and 2.1 mm. Period  $\Delta$  comprised the gradient pulse and a short delay (10  $\mu\text{s}$ ) on both side of the gradient pulse, and its length was  $200 \mu\text{s} + 2 \times 10 \mu\text{s} = 220 \mu\text{s}$ . Data was processed with an in-house MATLAB program.

The gas flowing through the channel was a mixture of Xe (1%), N<sub>2</sub> (10%), and He (89%). The spin polarization of <sup>129</sup>Xe nuclei was optically enhanced to about 3% using a commercial polarizer (Amersham Health, Durham, NC). The flow rate of the gas from the polarizer was adjusted to be about 0.3 standard liters per minute (SLM) in order to obtain proper polarization. After the polarizer, the flow was divided into two branches: one led to the membrane holder and the other led to the atmosphere. This enabled us to obtain a slow enough flow rate through the sample so that the travel time through the membrane region was longer than the longest delay used in the diffusion experiment. The flow rate through the latter branch was controlled by a needle valve. The flow rate and pressure at the outlet of the sample were controlled by a needle valve and pressure gauge, with the pressure kept at about 5 atm. The flow rate and stability were monitored throughout the experiments by bubbling the gas coming from the sample through a small water column (7 mm in diameter; 2 cm in length), using an outlet opening of 1/32" (0.8 mm). The bubbles were detected with a fiber-optic counter that was interfaced via a digital input line to a computer that was running a LabView program to measure and log the rate of bubble formation. The absolute flow velocity in the flow channel used in all the experiments was determined from the  $z$  encoded TOF experiment described below.

### 3. Results

**$z$  Encoded TOF Experiments.** In order to determine the flow rate of the gas in the flow channel,  $z$  (direction parallel to the flow direction) encoded TOF images<sup>18</sup> were measured from the samples. The pulse sequence is shown in Figure 3a. The experiment began with a  $\pi/2$  rf pulse followed by the labeling of spin coherences by a magnetic field gradient pulse in the  $z$  direction. The coherences were then stored as longitudinal magnetization by applying another  $\pi/2$  rf pulse in order to prevent dephasing during the flow to the detector. The amplitude of the encoded  $z$  magnetization was read stroboscopically by a series of  $\pi/2$  rf pulses in the detection coil.

The TOF flow images are shown in Figure 3b,c. From the images it can be seen that the atoms located close to the outlet of the channel ( $z = 3.5$  cm) during the encoding step arrive first in the detection coil, and that TOF increases linearly with increasing distance to the detection coil. The nonlinearity of the TOF curve above  $z = 3.5$  cm is a consequence of a narrowing in the flow channel at the point where the gas arrives in the outlet tubing. On the basis of the slopes in the membrane region, we calculated that the flow rates in these two experiments were  $3.93 \pm 0.07$  and  $3.85 \pm 0.06$  cm/s for the 20 and 200 nm pore membranes, respectively. On the basis of monitoring the relative flow rate by determining the rate of bubble formation with the fiber-optic detector, the flow rate in all the other

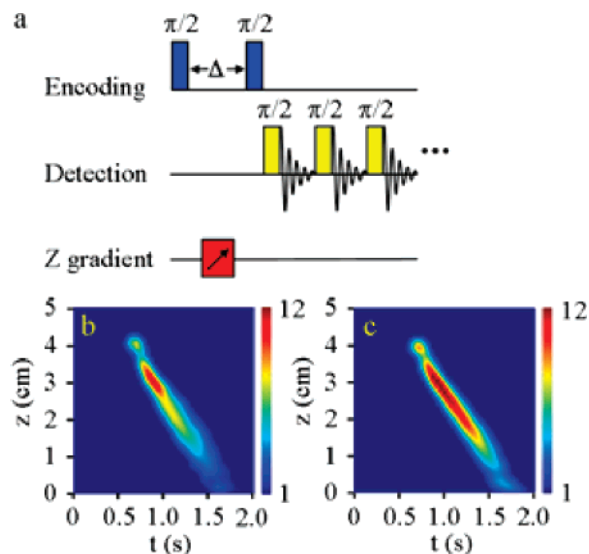


**Figure 3.** The pulse sequence of the  $z$  encoded experiment (a), and  $z$  encoded TOF images for the membranes containing (b) 20 nm and (c) 200 nm pores. Resolution in the  $z$  dimension is 2.1 mm (24 gradient steps). 32 transients were acquired in a total experiment time of 26 min. Zero filling was applied in the  $z$  dimensions so that, after the filling, the total number of points was doubled.

experiments was set to the same value as in these calibration experiments. The width of the TOF curve increases with increasing  $t$  because of hydrodynamic dispersion. The dispersion seems to be higher in the sample containing the 20 nm pore membrane.

**$yz$  Encoded TOF Experiments.** Extension of the previous TOF imaging experiment to two spatial dimensions by applying encoding gradients in two different orthogonal directions gives more detailed insight into the flow inside the channel.<sup>18</sup> The encoding directions used in the experiments were  $y$  (perpendicular to the surface of the membrane) and  $z$  (parallel to the flow direction). The pulse sequence is shown in Figure 4a.

The TOF flow images are shown in Figure 4b,c. The amplitude in the middle of the channel in the time projections is weak because the center pixels are partially filled with membrane. The Reynolds number in the subchannels separated by the membrane is very low ( $\sim 40$ ), indicating laminar flow. However, because the diffusion of gas across the subchannel ( $\sim 20$  ms for 0.5 mm) is fast compared with the travel times ( $\sim$ seconds), the average TOF does not depend on the lateral position of the gas atoms during the encoding, and therefore the amplitude in the individual panels does not show the stereotypic parabolic flow profile.<sup>28</sup> Above the end of the membrane region ( $z = 3.5$  cm), the gas begins to flow coherently in the undivided channel, and the amplitude gap is no longer seen in the center of the channel. The narrowing of the flow channel in that region can also be seen from the flow profile.

**$yy$  Encoded Diffusion Experiments.** The experiment used for measuring diffusion across the membrane contains two  $y$  (direction perpendicular to the surface of the membrane) encoding steps separated by a small delay. As the spin state is preserved during the delay, the experiment allows correlation of the initial position with the final position of an ensemble of fluid atoms inside the flow channel, and therefore it shows whether xenon atoms diffuse through the membrane during the delay. The experiment thus makes it possible to determine the diffusion rate, as the following elucidation shows (see also Figure 5): Consider that the labeling of the molecules during the first encoding step means that the molecules become red or

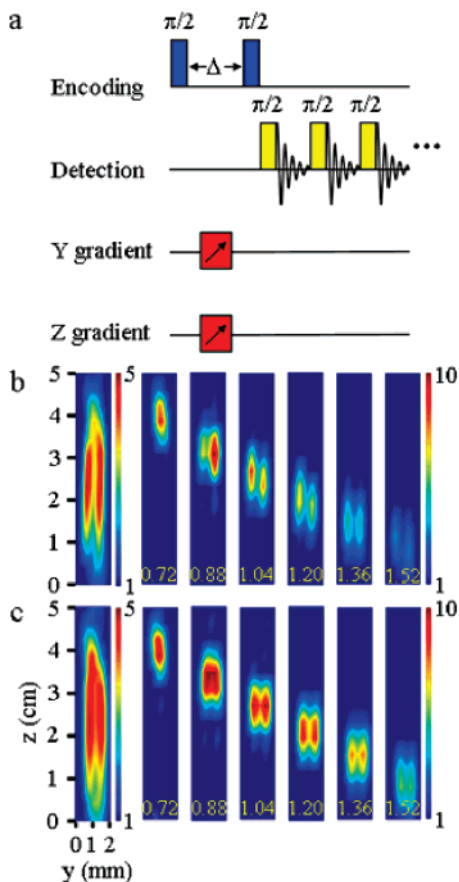


**Figure 4.** The pulse sequence of the  $yz$  encoded experiment (a), and  $yz$  encoded TOF images for the membranes containing (b) 20 nm and (c) 200 nm pores. The left-hand side pictures in panels b and c are sums of all the images measured at different travel time instants. The other images are the averages of the measurements of three successive travel times. The resolutions in the  $y$  and  $z$  dimensions are 0.3 and 7.1 mm (seven gradient steps in both directions). The average travel time in seconds is shown in the panels. 32 transients were acquired in a total experiment time of 53 min. Zero filling was applied in both spatial dimensions so that, after the filling, the total number of points was doubled.

blue depending on in which side of membrane they are (Figure 5b). Now we have an *apparent* concentration gradient of the red and blue molecules across the membrane. Subsequently, the molecules can diffuse through the membrane, and the concentration gradient decreases (Figure 5c). The rate of decrease depends on the diffusion rate. Consider that the second encoding changes the color of the molecules that are now on a different side of the membrane than during the first encoding step (red to violet and blue to green), whereas the other molecules maintain the initial color (Figure 5d). The signals of the red and blue molecules appear in the lower left and upper right quadrant, those of the violet and green molecules appear in the upper left and lower right quadrant of the correlation image (Figure 5e), and their amplitudes are proportional to the concentrations of the corresponding molecules. Because the concentrations of red and blue or violet and green molecules represent the portion of the molecules being on the same or different side of the membrane, respectively, before and after the delay and because the diffusion time and initial concentration gradient is known, the diffusion constant characterizing the diffusion rate can be calculated from the amplitudes, as will be shown later. The amplitudes of the signals in the correlation images also reveal the anisotropy of the diffusion, i.e., whether the diffusion in one direction is faster than in the other.

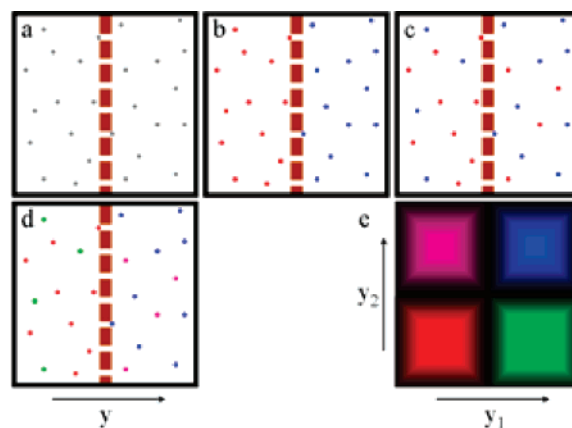


**Figure 5.** Measuring diffusion across a membrane by double phase encoded MRI method. (a) Before the first encoding step, the fluid molecules contain no information, and therefore they are represented by gray dots. (b) During the first encoding step, the initial position of the molecules in the direction perpendicular to the surface of the membrane ( $y$  direction) is encoded to spin coherences, and therefore the molecules on the left and right sides of membrane are represented by red and blue dots, respectively. (c) During the delay between the encoding steps, molecules diffuse across the membrane. (d) During the second encoding step, positional information of the molecules is encoded again to spin coherences, and, because the spin state preserves during the delay, the molecules now contain information of their initial and final positions. Therefore, the molecules on the left (right) during both encoding steps are represented in red (blue), and those moving from left (right) to right (left) are violet (green). (e) Resulting position correlation image.  $y_1$  and  $y_2$  are the  $y$  positions during the first and second encoding steps, respectively. The colors correspond to the colors used in panel d. The relative amplitude of violet and green signals shows how a large amount of molecules diffuses across the membrane during the delay.

In our system, the width of the channel divided by the membrane was made small (1.2 mm) in order to get the bulk diffusion time across the half channel shorter than the diffusion time across the membrane. This makes it easier to distinguish the effect of membrane from bulk diffusion. The membrane assembly requires a certain amount of space, and technically it would be very difficult to decrease the membrane holder size below the centimeter scale. This fact causes a sensitivity problem, because the filling factor of the probe fluid inside the coil is very low. Consequently, instead of conventional detection, we ended up using the remote detection technique, which enabled us to detect the signal outside the sample with a much smaller and more sensitive coil with optimized filling factor.

The pulse sequence for the double  $y$  encoded experiment is shown in Figure 6a. The first two rf pulses and the gradient pulse between them represent the first encoding step, including the storage of one component of the magnetization in the longitudinal direction in order to prevent dephasing during the delay  $\tau$ . The delay is followed by the second phase encoding step, after which the magnetization is stored again as longitudinal magnetization. Contrary to the PGSTE experiment, the gradients in the first and second encoding steps are ramped independently. Subsequent to the encoding sequence, the fluid flows to the detector, and the amplitude of the longitudinal magnetization modulated by both encoding steps is detected stroboscopically by a train of  $\pi/2$  rf pulses.

In order to obtain quadrature detection (QD) in each dimension and to destroy the signal of unencoded atoms, a 16-step phase cycling of the pulses and receiver is applied in the experiment. An implementation is shown in Table 1. The experiment performed with this phase cycling mimics a directly detected experiment in which a  $\pi/2$  pulse is followed by the

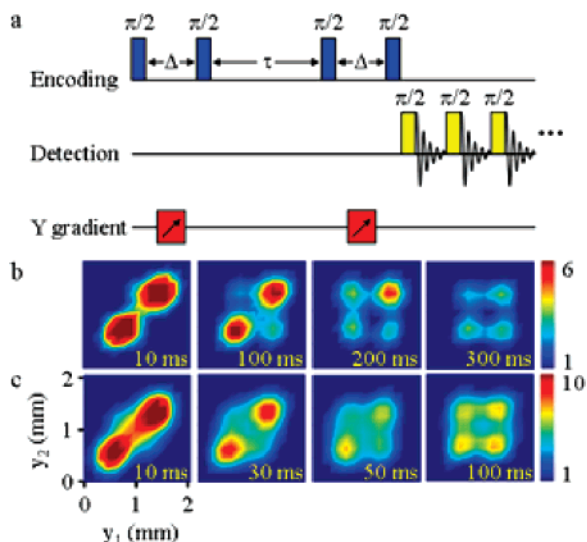


**Figure 6.** The pulse sequence of the  $yy$  encoded experiment (a) and  $y$  correlation images measured for the membranes containing (b) 20 nm and (c) 200 nm pores. In the images, 10 successive TOF transients were summed in order to increase the SNR. The transients were selected so that the images contain signal only from the region of the channel containing the membrane (between  $z = 0.5$  and  $3.5$  cm). The delays  $\tau$  used in the experiments are shown in the images. The resolution in both  $y$  dimensions is 0.3 mm (7 gradient steps). 64 transients were acquired in a total experiment time of about 2 h. Zero filling was applied in both spatial dimensions so that, after the filling, the total number of points was doubled.

**TABLE 1: Sixteen-Step Phase Cycling Used in the  $yy$  Encoded Experiment**

$m^a$	$\phi_{\text{enc}1}^b$	$\phi_{\text{enc}2}$	$\phi_{\text{enc}3}$	$\phi_{\text{enc}4}$	$\phi_{\text{det}}^c$	$\phi_{\text{rec}}^d$
0	$x$	$x$	$x$	$x$	$x$	$x$
1	$x$	$x$	$x$	$y$	$y$	$x$
2	$x$	$y$	$x$	$x$	$y$	$x$
3	$x$	$y$	$x$	$y$	$-x$	$x$
4	$x$	$-x$	$x$	$x$	$x$	$-x$
5	$x$	$-x$	$x$	$y$	$y$	$-x$
6	$x$	$-y$	$x$	$x$	$y$	$-x$
7	$x$	$-y$	$x$	$y$	$-x$	$-x$
8	$x$	$x$	$x$	$-x$	$x$	$-x$
9	$x$	$x$	$x$	$-y$	$y$	$-x$
10	$x$	$y$	$x$	$-x$	$y$	$-x$
11	$x$	$y$	$x$	$-y$	$-x$	$-x$
12	$x$	$-x$	$x$	$-x$	$x$	$x$
13	$x$	$-x$	$x$	$-y$	$y$	$x$
14	$x$	$-y$	$x$	$-x$	$y$	$x$
15	$x$	$-y$	$x$	$-y$	$-x$	$x$

<sup>a</sup>  $m$  is the cycle counter. <sup>b</sup>  $\phi_{\text{enc}1}$  refers to the phase of the first encoding pulse,  $\phi_{\text{enc}2}$  refers to the second, etc. <sup>c</sup>  $\phi_{\text{det}}$  is the phase of all the detection pulses in one cycle. <sup>d</sup>  $\phi_{\text{rec}}$  is the phase of the receiver.

first and second encoding gradient and the signal detection without any delays and storage pulses; the same product operator terms are collected and summed together in the  $yy$  encoded remote detection experiment after applying the first four steps of the phase cycling scheme in the table. This assures QD in each dimension. In addition, the phases of the second and fourth encoding pulses as well as the detection pulses are inverted in order to remove the signal of unencoded atoms. These operations lead to  $4 \times 4 = 16$  cycles altogether.

Figure 6b,c shows the correlations between the  $y$  values of  $y_1$  and  $y_2$  in the first and second encoding steps, respectively, measured by the  $yy$  encoded method. The amplitude of any  $[y_1, y_2]$  pixel in the image is proportional to the probability of an atom to be situated in an  $xz$  slice at  $y_1$  during the first encoding step and in the slice at  $y_2$  during the second step. Because the

membrane is located at  $y \approx 1.0$  mm, the nonzero amplitude of the pixels at  $y_1 < 1.0$  mm and  $y_2 > 1.0$  mm (upper left quadrant) or at  $y_1 > 1.0$  mm and  $y_2 < 1.0$  mm (lower right quadrant) shows unambiguously that a part of the fluid molecules passes through the membrane.

In the case of the shortest delay ( $\tau = 10$  ms), the amplitude of the signals in the upper left or lower right quadrants (referred to as cross-peaks hereafter) is almost zero, indicating that the diffusion through the membrane is insignificant during  $\tau$ . However, the width of the signals around the diagonal in the lower left and upper right quadrants (referred to as diagonal peaks hereafter) shows that significant diffusion across the subchannels takes place during the delay. When  $\tau$  is increased, the cross-peaks begin to grow, evidencing the transport of xenon gas through the membrane. The amplitude of the cross-peaks increases more rapidly with increasing  $\tau$  for the 200 nm membrane than for the 20 nm membrane, showing that the diffusion through the former membrane is faster than that through the latter one. The sum of the amplitudes of all the peaks decreases with increasing  $\tau$  because of dispersion during  $\tau$ . This behavior is more remarkable in the images of the 20 nm membrane than in those of the 200 nm membrane, because the longest delay is much longer in the former case (300 ms) than in the latter case (100 ms).

In order to analyze the correlation images, we need to have a model that correlates the behavior of amplitudes of the signals with the diffusion constant representing the diffusion rate through a membrane. According to Fick's law of diffusion, the current density,  $j$  (mol/m<sup>2</sup>s), along the  $y$ -axis is directly proportional to the change in concentration per unit length,  $dC/dy$  (mol/m<sup>4</sup>):

$$j = -D \frac{dC}{dy} \quad (1)$$

The proportionality coefficient  $D$  (m<sup>2</sup>/s) is the diffusion coefficient. Assuming that  $j$  is independent of  $y$  and  $D$  is constant, Fick's law can be modified in the form

$$j = D \frac{C_0 - C}{y} \quad (2)$$

where  $C_0$  and  $C$  are concentrations at  $y = 0$  and  $y = y$ . Consider the diffusion across the membrane in a  $yy$  encoded experiment. The membrane divides the flow channel into two subchannels, 1 and 2 (left and right part in Figure 5a). Immediately after the first encoding step, the concentration of xenon atoms encoded on subchannel 1 (red dots in Figure 5b) is zero on subchannel 2, and therefore the rate of net diffusion,  $R$  (mol/s), of those atoms across the membrane is

$$R = jA = \frac{DCA}{t_m} \quad (3)$$

where  $C$  is the concentration of the encoded atoms on subchannel 1,  $A$  is the surface area of the membrane, and  $t_m$  is the thickness of the membrane (60  $\mu$ m in this case). Assuming that the membrane is the main barrier to diffusion in the sample, that is, the diffusion across the subchannel is much faster than the diffusion through the membrane, the change of the concentration of the atoms encoded in subchannel 1 on subchannel 2 per unit time due to diffusion is

$$\frac{dC}{d\tau} = \frac{R}{V} \quad (4)$$

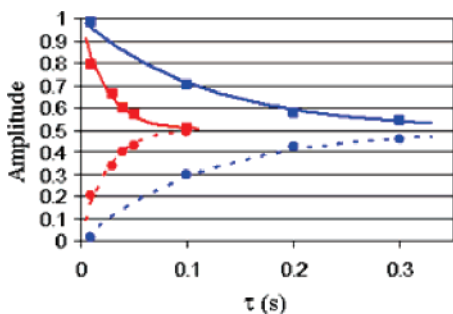


**Figure 7.** Amplitudes of diagonal (squares) and cross- (circles) peaks of the samples containing 20 (blue) and 200 nm (red) pores. Solid and dashed lines are least-squares adjustments of eqs 7 and 8, respectively, to the data points.

where  $V$  is the volume of the subchannel.  $V$  can be written as  $V = Aw_s$ , where  $w_s$  is the width of the subchannel (0.6 mm in this case). Let  $C_{ij}(\tau)$  be the concentration of atoms that were initially in subchannel  $i$ , and are now in subchannel  $j$  at time  $\tau$ . On the basis of the diffusion rates, the following equations can be derived:

$$\frac{dC_{ii}}{d\tau} = \frac{D}{w_s t_m} (-C_{ii} + C_{ik}) \quad (5)$$

$$\frac{dC_{ik}}{d\tau} = \frac{D}{w_s t_m} (-C_{ik} + C_{ii}) \quad (6)$$

Here,  $i = k = 1, 2$  and  $i \neq k$ . ( $C_{11}$ ,  $C_{22}$ ,  $C_{12}$  and  $C_{21}$  correspond to the concentrations of the red, blue, violet, and green dots in Figure 5d, respectively.) At  $\tau = 0$ ,  $C_{ii} = C$  and  $C_{ik} = 0$ . Concentrations  $C_{ii}(\tau)$  and  $C_{ik}(\tau)$  can be solved on the basis of previous equations, and, because the amplitude of the diagonal peaks,  $a_{\text{diag}}$ , is proportional to  $C_{ii}$  and that of the cross-peaks,  $a_{\text{cross}}$ , is proportional to  $C_{ik}$ , after the normalization  $a_{\text{diag}} + a_{\text{cross}} = 1$ , we obtain

$$a_{\text{diag}} = \frac{1}{2} \left[ 1 + \exp\left(-\frac{2D\tau}{w_s t_m}\right) \right] \quad (7)$$

and

$$a_{\text{cross}} = \frac{1}{2} \left[ 1 - \exp\left(-\frac{2D\tau}{w_s t_m}\right) \right] \quad (8)$$

The integrated amplitudes of the diagonal and cross-peaks together with the least-squares adjustments of eqs 7 and 8 to the data points are shown in Figure 7. The adjustments result in  $D$  values of  $(1.54 \pm 0.07) \times 10^{-7}$  m<sup>2</sup>/s for the 20 nm membrane and  $(7.5 \pm 0.2) \times 10^{-7}$  m<sup>2</sup>/s for the 200 nm membrane. The fit is excellent, which is reflected in the small errors in the obtained diffusion constants. The diffusion constant is proportional to both the diffusion rate *inside* the pores and the probability of the molecules to enter the pores, which in turn is proportional to the surface porosity. The diffusion constant is about 5 times larger for the membrane containing larger pores, even though its surface porosity is smaller (25–30% vs 50%), indicating that the diffusion in the 200 nm pores is much faster than that in the 20 nm pores.

The effect of relaxation is not taken into account in eqs 7 and 8. However, the relaxation time of bulk xenon gas is on the order of minutes, which is much longer than the travel times (~1 second). In addition, the relaxation time of xenon inside the pores is much longer (on the order of seconds) than the

diffusion time of xenon through the pores (on the order of 10 ms on the basis of previous results). Therefore, the effect of relaxation should be negligible.

#### Sensitivity Enhancement Obtained by Remote Detection.

Here we estimate the enhancement of the signal-to-noise ratio (SNR) in a remotely detected  $yy$  encoded TOF experiment when compared with a corresponding experiment detected by the encoding coil immediately after the last gradient pulse.

The theoretical sensitivity ratio,  $\Lambda$ , of the detection and encoding coil is<sup>29</sup>

$$\Lambda = \frac{t_{90}^e}{t_{90}^d} \quad (9)$$

where  $t_{90}^d$  and  $t_{90}^e$  are the lengths of the  $\pi/2$  pulses for the encoding and detection coils, respectively. On the basis of experimentally determined pulse lengths,  $\Lambda$  is 100 in our case. The volumes of xenon gas inside the encoding ( $V_e$ ) and detection ( $V_d$ ) coils are about 40 mm<sup>3</sup> and 2.5 mm<sup>3</sup>, respectively. Theoretical SNR enhancement of the xenon signals measured directly by the coils is

$$\Lambda \frac{V_d}{V_e} = 100 \cdot \frac{2.5 \text{ mm}^3}{40 \text{ mm}^3} = 6.3$$

The measured enhancement is 6.9, which is in agreement with the theoretical estimation.

Assuming that all the encoded xenon atoms are detected in the  $yy$  encoded remote detection experiment by optimizing the delay between detection pulses so that, between the pulses, all the atoms detected previously have left the detection coil volume, and the volume is filled by undetected atoms, the number of FID signals collected in a remote detection experiment is  $V_e/V_d = 16$ . If these signals are summed together, the SNR enhancement is

$$\sqrt{16} \cdot 6.9 = 27.6$$

One component of the magnetization vector is always lost when the spin coherences are stored as a longitudinal magnetization, and, contrary to the remotely detected experiment, the direct experiment does not require storing after the second phase encoding step. This fact leads to the decrease of the relative SNR by a factor of  $\sqrt{2}$ . Therefore, the total theoretical SNR enhancement in a  $yy$  encoded TOF experiment is about 20 as compared to the corresponding directly detected experiment. In the previous calculation, the effect of dispersion, which may slightly decrease the obtained SNR enhancement, is neglected.

## 4. Discussion

The double encoded MRI experiment introduced here may be viewed as a stimulated echo variant of the position exchange spectroscopy (POXSY) experiment<sup>30</sup> containing some of the additional modifications needed in remote detection. In principle, the measurements could be done using the POXSY pulse sequence. However, like in the related PGSE experiment, the relaxation attenuation of the signal is dominated by  $T_2$  in the POXSY experiment. Membrane systems contain a large surface area per unit volume, and  $T_2$  is usually much shorter than  $T_1$  because of local magnetic susceptibility variations along interfaces. Therefore, an experiment dominated by  $T_2$  relaxation is unfavorable for measuring the diffusion across a membrane. However, the relaxation attenuation of the signal is dominated

by  $T_1$  in the experiment introduced here, and it enables using the relatively long delays required in the diffusion experiments.

Even though the double encoded MRI experiment can also be done in a conventional way without using another coil for detection, the sensitivity enhancement obtained by remote detection is crucial when the diffusion of *gas* across a membrane is studied. We estimated above that, in the present setup, the SNR per unit time is about 20 times larger than in the corresponding directly detected experiment. Because the  $\gamma\gamma$  encoded remote detection experiment took about 2 h, the direct experiment using the same setup with the same SNR would take about 1 month, which is unfeasible. A smaller coil around the sample would increase the relative sensitivity of the directly detected experiment, but the membrane assembly always requires a certain amount of space, and technically it would be very difficult to decrease the membrane holder size below centimeter scale. A large coil allows for an increased experimental flexibility, particularly for measuring diffusion in technologically relevant devices, such as membrane filter elements, and, because the size of the encoding coil does not affect the sensitivity of remote detection, it is advantageous to use this detection technique to measure diffusion.

In this demonstration, we used a gas mixture containing a small amount of hyperpolarized xenon. However, experiments with thermally polarized gases are also possible, and indeed may give higher SNRs than the present xenon experiments if the molecules contain several chemically equivalent spins with large gyromagnetic ratios,  $\gamma$ . For example, consider an equivalent experiment done with pure propane gas. Even though the polarization of hyperpolarized xenon (3%) is about 1300 times the thermal polarization of protons in a 300 MHz field at room temperature, six chemically equivalent nuclei of the methyl groups, the 4-fold natural abundance of  $^1\text{H}$  as compared with  $^{129}\text{Xe}$ , the detection of nuclei with higher gyromagnetic ratios ( $\text{SNR} \propto |\gamma|^{3/2}$ ), and the fact that there is only 1% of xenon in the gas mixture that was used increases the relative sensitivity of propane by a factor of 16 000. Therefore, the SNR of the propane experiment can be estimated to be about 12 times better than that of the xenon experiment. However, the short  $T_1$  relaxation time (about  $1.9 \text{ s}^{31}$ ) of propane decreases the relative sensitivity by a factor of 3, if travel time is 2 s, and therefore it can be concluded that the sensitivity of the propane experiment would be about 4 times better than that of the xenon experiment.

Naturally, the method presented here is also suitable for studying the diffusion of *liquids* through the membranes. It was shown that remotely detected measurements are also possible when a liquid is used as a probe fluid.<sup>18</sup> However, because the NMR signal of liquids is much stronger than that of gases because of the higher spin density, it may be even possible to use a directly observed experiment in this case. For instance,  $^1\text{H}$  spin density in water is about 100 times larger than that in 5 atm of propane, meaning a 100 times larger relative NMR sensitivity, and this should enable the direct detection by the coil around the sample in the current setup. On the other hand, because the diffusion constant of liquids is much smaller than that of gases, the width of the membrane channel may have to be smaller in order to get fast enough diffusion rate across the subchannels, and this fact may decrease the sensitivity of the experiment.

## 5. Conclusions

It has been shown that an MRI experiment containing two encoding steps separated by a delay can be used for the quantitative analysis of diffusion through a membrane. The

experiment is noninvasive; it does not require the introduction of foreign tracers or partial pressure or concentration gradients across the membrane, the manipulation of nuclear spin coherences does not affect the molecular interactions and transport, and the radio frequency radiation used in MRI is also capable of penetrating inside opaque materials without damaging the sample. This method also makes it possible to measure self-diffusion of the molecules across a membrane under equilibrium conditions. The double encoding can be realized by the POXSY experiment based on the spin-echo sequence<sup>30</sup> or by its stimulated echo-based counterpart introduced here. The relaxation behavior in the membrane systems makes the latter option favorable. This position correlation experiment is advantageous also in other diffusion experiments, because, contrary to PGSE type experiments, the correlation image reveals directly the propagator of the molecules.

Applied to membranes, the experiment exhibits low sensitivity as a result of geometric constraints leading to a poor filling factor. We demonstrated here that the sensitivity problem can be overcome by the remote detection technique, in which the spatial information is encoded in the spin coherences by a large coil around the sample, and the signal is detected by a much smaller and more sensitive coil in a different location. Because the size of the encoding coil does not affect the sensitivity, remote detection increases the experimental flexibility, making it possible to measure diffusion in complete devices. The encoding can be done even in a lower magnetic field if the material of the sample is not compatible with a high magnetic field.<sup>17</sup>

In principle, all the NMR active fluids can be used as a probe fluid. However, in the case of gases, the sensitivity limits the candidates, and it is favorable to use hyperpolarized gases or thermally polarized gases with the molecules containing several chemically equivalent spins with a large gyromagnetic ratio. The sensitivity is not a serious problem when liquids are used as a probe fluid, because they yield a strong NMR signal due to the high spin density.

The experiment presented here can be used for several purposes. A few examples are as follows: The diffusion properties among different membranes can be compared by using the same probe fluid (e.g., xenon) for all the samples. It is also possible to study the diffusion properties of different fluids in the same membrane system, if the fluids contain NMR active molecules. Furthermore, because of the use of noninvasive MRI encoding combined with the highly sensitive remote detection of the signal, this experiment allows characterizing membrane diffusion and transport in intact systems of technological importance, such as fuel cells and gas separation systems.

**Acknowledgment.** The authors thank Dr. Josef Granwehr for helpful discussions. This work was supported by the Director, Office of Science, Office of Basic Energy Sciences, Materials Sciences and Nuclear Science Divisions, of the U.S. Department of Energy under Contract DE-AC03-76SF00098. V.-V.T. acknowledges the Academy of Finland for financial support. E.H. is supported by a fellowship from the U.S. Department of Homeland Security under DOE Contract Number DE-AC05-00OR22750.

## References and Notes

- (1) Kordesch, K.; Simader, G. *Fuel Cells and Their Applications*; VCH: New York, 2001.
- (2) Singh, R. *Hybrid Membrane Systems for Water Purification*; Elsevier: Oxford, 2006.

- (3) Vieth, W. R. *Diffusion in and through Polymers*; Hanser Verlag: Munich, Germany, 1991.
- (4) Höfer, M. *Transport Across Biological Membranes*; Pitman Publishing: Marshfield, MA, 1981.
- (5) Crank, J.; Park, G. S., Eds. *Diffusion in Polymers*; Academic Press: New York, 1968.
- (6) Stejskal, E. O.; Tanner, J. E. *J. Chem. Phys.* **1965**, *42*, 288.
- (7) Tanner, J. E. *J. Chem. Phys.* **1970**, *52*, 2523.
- (8) Callaghan, P. T. *Principles of Nuclear Magnetic Resonance Microscopy*; Clarendon Press: Oxford, 1991.
- (9) Kimmich, R. *NMR – Tomography, Diffusometry, Relaxometry*; Springer: New York, 1997.
- (10) Kärger, J. *Diffusion in Zeolites and Other Microporous Solids*; John Wiley & Sons: New York, 1992.
- (11) Callaghan, P. T.; Coy, A.; MacGowan, D.; Packer, K. J.; Zelaya, F. O. *Nature* **1991**, *351*, 467.
- (12) Kärger, J.; Heink, W. *J. Magn. Reson.* **1983**, *51*, 1.
- (13) Callaghan, P. T.; Jolley, K. W.; Humphrey, R. S. *J. Colloid Interface Sci.* **1983**, *93*, 521.
- (14) Mitra, P. P.; Sen, P. N.; Schwartz, L. M.; Le Doussal, P. *Phys. Rev. Lett.* **1992**, *68*, 3555.
- (15) Mitra, P. P.; Sen, P. N. *Phys. Rev. B* **1992**, *45*, 143.
- (16) Latour, L. L.; Mitra, P. P.; Kleinberg, R. L.; Sotak, C. H. *J. Magn. Reson., Ser. A* **2003**, *101*, 342.
- (17) Moule, A. J.; Spence, M.; Han, S.; Seeley, J.; Pierce, K.; Saxena, S.; Pines, A. *Proc. Natl. Acad. Sci. U.S.A.* **2003**, *100*, 9122.
- (18) Granwehr, J.; Harel, E.; Han, S.; Garcia, S.; Pines, A. *Phys. Rev. Lett.* **2005**, *95*, 075503.
- (19) Harel, E.; Granwehr, J.; Seeley, J.; Pines, A. *Nat. Mater.* **2006**, *5*, 321.
- (20) Hilty, C.; McDonnell, E.; Granwehr, J.; Pierce, K.; Han, S.; Pines, A. *Proc. Nat. Acad. Sci. U.S.A.* **2005**, *102*, 14960.
- (21) Harel, E.; Hilty, C.; Koen, K.; McDonnell, E.; Pines, A. *Phys. Rev. Lett.* **2007**, *98*, 017601.
- (22) Xu, S.; Yashchuk, V. V.; Donaldson, M. H.; Rochester, S. M.; Budker, D.; Pines, A. *Proc. Natl. Acad. Sci. U.S.A.* **2006**, *103*, 12668.
- (23) Ratcliffe, C. I. *Annu. Rep. NMR Spectrosc.* **1998**, *36*, 123.
- (24) Walker, T. G.; Happer, W. *Rev. Mod. Phys.* **1997**, *69*, 629.
- (25) Goodson, B. M. *J. Magn. Reson.* **2002**, *155*, 157.
- (26) Han, S.; Granwehr, J.; Garcia, S.; McDonnell, E. E.; Pines, A. *J. Magn. Reson.* **2006**, *182*, 260.
- (27) McDonnell, E. E.; Han, S.; Hilty, C.; Pierce, K. L.; Pines, A. *Anal. Chem.* **2005**, *77*, 8109.
- (28) Taylor, G. I. *Proc. R. Soc. A* **1953**, *219*, 186.
- (29) Hoult, D. I.; Richards, R. E. *J. Magn. Reson.* **1976**, *24*, 71.
- (30) Han, S.; Stapf, S.; Blümich, B. *J. Magn. Reson.* **2000**, *146*, 169.
- (31) Hirasaki, G. J.; Lo, S.-W.; Zhang, Y. *Magn. Reson. Imaging* **2003**, *21*, 269.